Osteoblast AMP-activated protein kinase regulates postnatal skeletal development in male mice

Ippei Kanazawa, Ayumu Takeno, Ken-ichiro Tanaka, Masakazu Notsu, and Toshitsugu Sugimoto

Internal Medicine 1, Shimane University Faculty of Medicine, 89-1, Enya-cho, Izumo, Shimane, 693-8501, Japan

Short title: AMPK and Bone development

Key words: AMP-activated protein kinase, osteoblast, RANKL, BMP-2, osterix

Correspondence and requests for reprints:

Ippei Kanazawa, MD, PhD

Internal Medicine 1, Shimane University Faculty of Medicine, 89-1, Enya-cho, Izumo, Shimane, 693-8501, Japan

Phone: +81-853-20-2183, Fax: +81-853-23-8650

E-mail: ippei.k@med.shimane-u.ac.jp

Grant: This study was partly supported by a Grant-in-Aid for Scientific Research (C)

19 (15K09433).

20 **Disclosure Summary:** The authors have nothing to disclose.

Abstract

Studies have shown that AMP-activated protein kinase (AMPK), a crucial regulator of energy homeostasis, plays important roles in osteoblast differentiation and mineralization. However, little is known about *in vivo* roles of osteoblastic AMPK in bone development. Thus, to investigate *in vivo* roles of osteoblast AMPK, we conditionally inactivated *Ampk* in osterix (Osx)-expressing cells by crossing Osx-Cre mice with floxed AMPKα1 to generate mice lacking AMPKα1 in osteoblasts ($Ampk^{-/-}$ mice). Compared with wild-type and $Ampk^{+/-}$ mice, $Ampk^{-/-}$ mice displayed retardation of postnatal bone development, although bone deformity was not observed at birth. Micro-CT showed significant reductions in trabecular bone volume, cortical bone length and density, and increased cortical porosity in femur as well as development defects of skull in 8-week-old $Ampk^{-/-}$ mice. Surprisingly, histomorphometric analysis demonstrated that the number of osteoclasts was significantly increased, although bone formation rate was not altered. Loss of trabecular network connections and mass, as well as shortened growth plates and reduced thickness of cartilage adjacent to the growth plate, were observed in $Ampk^{-/-}$ mice. In primary cultured osteoblasts from calvaria, the expressions of alkaline phosphatase, type 1 collagen, osteocalcin, bone morphogenetic protein-2, Runx2, and osterix were significantly inhibited in $Ampk^{-/-}$

39 osteoblasts, whereas the expression of receptor activator of nuclear kappa-B ligand
40 (RANKL) and the RANKL/osteoprotegerin ratio were significantly increased. These
41 findings indicate that osteoblastic AMPK plays important roles in bone development *in*
42 *vivo*, and that deletion of AMPK in osteoblasts decreases osteoblastic differentiation and
43 enhances bone turnover by increasing RANKL expression.

Introduction

AMP-activated protein kinase (AMPK) is a crucial regulator of energy and metabolic homeostasis at the cellular and whole-organism levels (1,2). AMPK is found in single-cell eukaryotes, such as the yeast *Saccharomyces cerevisiae* and the primitive protist *Giardia lamblia*, and considered to be a metabolic stress-sensing enzyme that plays key roles in regulating cellular and whole-body energy homeostasis (3). It is a highly conserved serine/threonine heterotrimeric protein, consisting of a catalytic α subunit and two regulatory β and γ subunits, and functions as a serine/threonine kinase. An increase in the cellular AMP/ATP ratio activates AMPK through the phosphorylation of the α subunit. Once activated, AMPK inactivates several metabolic enzymes involved in ATP-consuming cellular events, including cholesterol and protein synthesis (4). Accumulating evidence has indicated that AMPK is a candidate therapeutic target for metabolic disease, atherosclerosis, and cancer (4,5).

Previous studies have shown that the AMPK signaling pathway plays pivotal roles in bone physiology (6). AMPK subunits are expressed in bone tissue and cells, and the AMPKα1 subunit is the dominant catalytic isoform expressed in bone (7,8). We previously demonstrated that AMPK activation stimulated the differentiation and mineralization of osteoblasts by enhancing the expression of bone morphogenetic

protein-2 (BMP-2) and endothelial nitric oxide synthase via inhibition of HMG-CoA reductase (9–11). Moreover, other researchers reported that AMPK activation induced calcified nodule formation in primary osteoblasts, whereas AMPK inhibition suppressed the effects of AMPK and osteoblastic differentiation (12,13). These findings suggest that AMPK has an important function in the differentiation of osteoblasts and bone formation.

On the other hand, previous studies have shown that AMPK activation directly inhibits osteoclastogenesis (14,15). Furthermore, it is reported that AMPK activation indirectly suppresses osteoclast differentiation by stimulating osteoprotegerin (OPG) and reducing receptor activator of nuclear kappa-B ligand (RANKL) expression in osteoblasts (16). In addition, we recently showed that AMPK activation significantly decreased RANKL expression in osteocytic MLO-Y4 cells, and that knockdown of AMPKα1 significantly increased RANKL expression (8). These findings suggest that AMPK activation inhibits osteoclast activity directly and indirectly by decreasing RANKL expression in both osteoblasts and osteocytes. Thus, AMPK may play a pivotal role in osteoclastogenesis and bone remodeling.

Recently, a few studies using genetic mutant mice have shown that inactivation of AMPK decreases bone mass *in vivo* (7,12,17). Shah *et al.* generated conventional

AMPKα1 knockout mice and examined the bone phenotype by micro computed tomography (μCT). Both cortical and trabecular bone compartments were significantly smaller in AMPKα1 knockout mice compared to the wild-type littermates (12). Moreover, dynamic bone histomorphometric analysis showed increased bone turnover and bone resorption in the knockout mice compared with that of their wild-type (WT) littermates (17). Taken together, these findings suggest that AMPK may play important roles in bone development and remodeling. However, AMPK acts as a crucial regulator of whole body energy and metabolic homeostasis (1,2), which may affect bone metabolism. In addition, AMPK in osteocytes and osteoclasts may play important roles in bone development. Therefore, the roles of AMPK in osteoblasts are still unclear. In this study, to investigate *in vivo* roles of osteoblast AMPK, we conditionally inactivated AMPK by crossing osterix (Osx)-Cre mice with floxed AMPKα1 ($Ampk^{flox/flox}$) to generate mice lacking AMPKα1 in osteoblasts ($Ampk^{-/-}$ mice).

Materials and methods

Generation of knockout mice

A conditional knockout mouse model, in which the *Ampkα1* gene is deleted specifically in osteoblasts, was generated. *Ampkα1*$^{flox/flox}$ mice (18) and Osx-Cre transgenic (*Osx-Cre*$^{TG/+}$) mice (19) were obtained from The Jackson Laboratory. *Ampkα1*$^{flox/flox}$ mice were crossed with *Osx-Cre*$^{TG/+}$ mice to generate *Osx-Cre*$^{TG/+}$*;Ampkα1*$^{flox/+}$ (*Ampk*$^{+/-}$) mice. These mice were crossed with *Ampkα1*$^{flox/flox}$ mice to generate litters that contained ~1/4 *Osx-Cre*$^{TG/+}$*;Ampkα1*$^{flox/flox}$ mice, which were used for subsequent crosses. The control WT littermate mice were designated as *Ampk*$^{flox/flox}$ and the knockout mice as *Osx-Cre;Ampk*$^{flox/flox}$ (*Ampk*$^{-/-}$); both were on the C57BL/6J background. All mice, which were used in this study, were male. Mice were maintained in a pathogen-free standard animal facility, and experimental procedures were performed following an animal use protocol approved by the Animal Care and Use Committee of Shimane University Faculty of Medicine.

The genotypes of *Ampk*$^{-/-}$ and control mice were confirmed by RT-PCR. The PCR conditions were as follows: 28 cycles of denaturation at 95°C for 15 s, annealing at 60°C for 15 s, and elongation at 72°C for 30 s. This was performed on genomic DNA extracted from mouse tails using a proteinase K digestion kit (KAPA Biosystems, Woburn, MA, USA) as previously described (20). Genotyping was conducted using

primers described by the Jackson Laboratory to detect the AMPK floxed allele (forward 5′-CCCACCATCACTCCATCTCT-3′ and reverse 5′-AGCCTGCTTGGCACACTTAT-3′) and the Osx-Cre transgenes (forward 5′-GCGGTCTGGCAGTAAAAACTATC-3′ and reverse 5′-GTGAAACAGCATTGCTGTCACTT-3′). To test for the specific deletion of *Ampkα1* exon 3, genomic DNA isolated from different tissues was amplified using a combination of primers: A (5′-CCCACCATCACTCCATCTC-3′), B (5′-AGCCTGCTTGGCACACTTAT), and C (5′-ATTAAGGGTGAGCACAGACCAG). PCR of the recombinant Δ3 *Ampk* allele generates a 395-bp amplicon (primers A + C), and the $Ampk^{flox}$ allele generates a 296-bp amplicon (primers A + B).

μCT analysis

Mouse femurs and skulls, dissected free of soft tissue, were fixed in 70% ethanol. High resolution images were acquired with a microfocus X-ray CT system (Scan Xmate-L090, Comscantecno Co., Ltd., Yokohama, Japan). The X-ray source was set at 75 kV and 100 μA, and the samples were rotated 360°. Image resolution was fixed at a pixel size of 10.334 μm. The magnification was 9.677 and slice thickness was 10.334 μm. Three-dimensional measurements and structural analyses were performed

with custom software (TRI/3D-BON, Ratoc System Engineering, Kanagawa, Japan).

Bone histomorphometric analysis

Mouse femurs were dissected, fixed for 24 h in 4% formalin, dehydrated in a graded ethanol series, and embedded in methyl methacrylate resin; 3-μm sections were made. After staining with Von Kossa and toluidine blue, histomorphometric analyses were performed with a Histometry RT Camera (System Supply Co., Ltd., Nagano, Japan). For H&E and Safranin O stainings, decalcified femurs were embedded in paraffin and cut into 5-μm sections. The sections were stained using standard procedures. Images were taken at room temperature using a light microscope (BX53; Olympus, Tokyo, Japan), and examined under natural and polarized light and by fluorescence microscopy. Area of growth plate and mean width of cartilage adjacent to the growth plate were measured by using ImageJ.

Double calcein labeling

Calcein (Sigma) was dissolved in buffer (0.15 M NaCl, 2% $NaHCO_3$) and injected twice intraperitoneally (25 μg/g body weight) at 5 and 2 days before the mice were euthanized (20). Bones were harvested and embedded in plastic as described

above. Serial sections were cut, and the freshly cut surface of each section was viewed and imaged using fluorescence microscopy. The double calcein-labeled width was measured, and the mineral apposition rate (MAR = interlabel width/labeling period) and bone formation rate/bone surface (BFR/BS) were calculated. Calculations were made on a minimum of duplicate specimens from replicate mice in each group.

Osteoblast isolation from mouse calvaria

Osteoblasts from calvaria of individual 1-week-old *Ampk*$^{-/-}$ pups or their WT littermates were isolated as previously described (20). The bones were dissected free of sutures and subjected to 2 consecutive digestions at 37°C with shaking in αMEM (Gibco-BRL, Rockville, MD, USA) containing 0.1 mg/mL collagenase P (Roche Applied Science, Penzberg, Germany) and 0.25% trypsin/0.1% EDTA (Invitrogen, San Diego, CA, USA). The supernatant was discarded leaving the pieces of bone. Fresh digestion medium containing 0.2 mg collagenase P/mL was added, and calvaria were incubated at 37°C with vigorous shaking every 15 min for 45 min or until bone pieces began to fall apart. The bone pieces and cells were collected by centrifugation (1500 × *g*), washed with αMEM, and plated in a 10-cm dish with αMEM containing 10% FBS and 1% penicillin/streptomycin (Invitrogen). On the following day, images were taken

167 at room temperature using a light microscope (TS100; Nikon). After 4 days, the medium
168 was changed, and when the cells reached 80% confluency they were passaged to 6-well
169 plates (10^5 cells/well).
170
171 ***Bone marrow stromal cells (BMSC) isolation***
172 BMSC from femur of 8-week-old *Ampk*$^{-/-}$ mice or their control littermates were
173 isolated. The mouse femurs were dissected free of surrounding soft tissue. The bone
174 marrow was flushed with αMEM. After centrifuge (1,000 rpm for 5 min) to isolate the
175 cells from the extra soft tissue, the cells were plated in culture flasks with αMEM
176 containing 10% FBS and 1% penicillin/streptomycin, and non-adherent cells were
177 removed. The cell culture medium was replaced every 3 days, and the cells were seeded
178 in 6-well plates and cultured in 5% CO_2 at 37°C.
179
180 ***RT-PCR analysis to identify AMPK subunits***
181 To investigate the mRNA expression of AMPK subunits (α1 and α2) in primary
182 osteoblasts, we performed RT-PCR. Total RNA was extracted from the cultured cells
183 using Trizol reagent (Invitrogen) according to the manufacturer's recommended
184 protocol. We used 2 μg total RNA for the synthesis of single-stranded cDNA (cDNA

185 synthesis kit; Invitrogen). The following primers were used: *Ampkα1* forward, 5′-
186 CTCTATGCTTTGCTGTGTGG-3′ and *Ampkα1* reverse, 5′-
187 GGTCCTGGTGGTTTCTGTTG-3′; *Ampkα2* forward, 5′-
188 ACAGCGCCATGCATATTCCT-3′ and *Ampkα2* reverse, 5′-
189 TCCGACTGTCTACCAGGTAA-3′. The PCR conditions were as follows: 35 cycles of
190 denaturation at 95°C for 45 s, annealing at 60°C for 30 s, and elongation at 72°C for 1
191 min. The PCR products were separated by electrophoresis on a 1.8% agarose gel and
192 were visualized using ethidium bromide staining with ultraviolet (UV) light using an
193 electronic UV transilluminator (Toyobo Co. Ltd., Tokyo, Japan).
194
195 ***Quantification of gene expression by real time PCR***
196 SYBR green chemistry was used to determine mRNA expression levels.
197 Primers were used as previously described (8-11). Real time PCR was performed in a
198 25-μL reaction mixture containing 1 μL cDNA using an ABI PRISM 7000 (Applied
199 Biosystems, Waltham, MA). Double-stranded DNA-specific SYBR Green I was mixed
200 with the PCR buffer provided in the SYBR Green Real-Time PCR Master Mix (Toyobo
201 Co. Ltd.) to quantify the PCR products. PCR conditions were as follows: initial
202 denaturation at 95°C for 15 min, and 40 cycles of denaturation at 94°C for 15 s and

annealing and extension at 60°C for 1 min. The mRNA level of *36B4*, a housekeeping gene, was used to normalize the differences in the efficiency of RT.

Statistical analysis

Results are expressed as mean ± SE. Statistical differences between groups were determined using one-way ANOVA followed by Fisher's protected least significant difference. For all statistical tests, a p value of <0.05 was considered statistically significant.

Results

Growth retardation of Ampk$^{-/-}$ mice during postnatal development

To monitor the growth of *Ampk*$^{-/-}$ mice during postnatal development, we measured body weight every week and collected femurs from *Ampk*$^{-/-}$ and WT littermates at 8 weeks after birth. *Ampk*$^{-/-}$ mice were viable at birth and showed no apparent growth defects after 1 day (Fig. 1A) and 2 weeks (Fig. 1B). The mice then developed dwarfism, characterized by smaller body size and shorter limbs (Fig, 1D). Body weight of *Ampk*$^{-/-}$ mice at 8 weeks was significantly decreased by 25% compared to that of WT and *Ampk*$^{+/-}$ mice (Fig. 1C). Moreover, femur length and size of *Ampk*$^{-/-}$ mice were reduced compared to those of WT at 8 weeks (Fig. 1E and F). Although

222 serum levels of calcium, phosphorus, albumin, creatinine, and parathyroid hormone
223 (PTH) were measured and compared between *Ampk*$^{-/-}$ and WT mice at 8 weeks, no
224 differences in these levels were observed (Table 1). Specificity of *Ampk* knockout in
225 bone tissue of *Ampk*$^{-/-}$ mice was confirmed by PCR amplification of tissue genomic
226 DNA (Fig. 1G). To examine the efficiency of *Ampkα1* knockout in osteoblasts, we
227 performed quantification of *Ampkα1* expression in isolated primary osteoblasts from
228 calvaria and BMSC from femur (Fig. 1H). Almost 80% and 60% deletion in osteoblasts
229 and BMSC, respectively, was confirmed. These findings indicate that osteoblast AMPK
230 is required for postnatal bone growth.
231
232 ***Osteoblast-specific disruption of the Ampkα1 gene decreases bone mass and volume***
233 *Ampk*$^{-/-}$ mice had marked reductions in trabecular bone, compared to WT and
234 *Ampk*$^{+/-}$ mice, assessed by μCT (Fig. 2A). Trabecular bone volume/tissue volume
235 (BV/TV) was significantly reduced in *Ampk*$^{-/-}$ mice (Fig. 2B), and trabecular separation
236 (TbSp) and structure model index (SMI) were significantly increased (Fig. 2E and G).
237 Moreover, μCT images showed that the cortical bone size was remarkably reduced in
238 *Ampk*$^{-/-}$ mice (Fig. 3A). Center line length (Cntr.L) of cortical bone and bone density
239 were significantly decreased in *Ampk*$^{-/-}$ mice (Fig. 3B and E), whereas vessel volume

240 (Vv) and Vv/cortical bone volume (Cv) were significantly increased (Fig. 3F and G). In
241 addition, μCT images of skulls showed that smaller and thinner skulls were observed in
242 *Ampk*$^{-/-}$ mice compared to WT and *Ampk*$^{+/-}$ mice (Fig. 4A). Quantification of volume,
243 surface area, and thickness of interparietal bone indicated that skull formation was
244 significantly reduced in *Ampk*$^{-/-}$ mice than WT and *Ampk*$^{+/-}$ mice (Fig. 4B-D).

245 Representative pictures of toluidine blue staining showed the marked reduction
246 in trabecular bone compared to WT mice (Fig. 5A and B). Histomorphometric analysis
247 indicated trabecular bone volume, thickness, and number were significantly reduced in
248 *Ampk*$^{-/-}$ mice compared to those of WT (Fig. 5C-E). Osteoblast number was slightly
249 increased in *Ampk*$^{-/-}$ mice compared to those of WT although the difference did not
250 reach significance. Mineral apposition rate and bone formation rate (BFR) showed no
251 difference between *Ampk*$^{-/-}$ mice and WT (Fig. 5J-L). However, BFR was significantly
252 decreased at endosteal surface of cortical bone in *Ampk*$^{-/-}$ mice (Fig. 5M), whereas it
253 was significantly increased at periosteal surface (Fig. 5N). In contrast, osteoclast
254 number and osteoclast surface/bone surface increased significantly in *Ampk*$^{-/-}$ mice (Fig.
255 5M and N).

256 H&E and Safranin O staining showed the loss of trabecular network
257 connections and mass, as well as shortened growth plates at the femoral distal end, in

258 *Ampk*$^{-/-}$ mice (Fig. 6E, F and G) compared to those of WT (Fig. 6A, B and C).
259 Quantification of growth plate area indicated a significant reduction in *Ampk*$^{-/-}$ mice
260 compared to that of WT (Fig. 6I). The thickness of cartilage adjacent to the growth
261 plates was reduced in *Ampk*$^{-/-}$ mice (Fig. 6H) compared to that of WT (Fig. 6D).
262 Quantification of mean width of cartilage adjacent to the growth plate indicated a
263 significant reduction in *Ampk*$^{-/-}$ mice compared to that of WT (Fig. 6J). These findings
264 suggest the occurrence of delayed epiphyseal ossification.
265
266 ***Disruption of the Ampkα1 gene inhibited osteoblastic differentiation and increased***
267 ***RANKL expression***
268 Microscopic images showed that spindle-shaped osteoblast-like cells migrated
269 from collagenase-treated calvaria of WT mice (Fig. 7A), whereas round-shaped cells
270 were observed from calvaria of *Ampk*$^{-/-}$ mice (Fig. 7B), suggesting that migrated cells
271 from WT mice differentiated to mature osteoblasts, but differentiation of the cells from
272 *Ampk*$^{-/-}$ was inhibited. RT-PCR confirmed that the *Ampkα1* gene was knocked out in
273 isolated osteoblasts from *Ampk*$_{osb}$$^{-/-}$ mice (Fig. 7C). Real-time PCR showed that
274 expressions of *Alkaline phosphatase (Alp)*, *Type 1 collagen (T1c)*, *Osteocalcin*, *Bmp-2*,
275 *Runx2*, and *Osterix* were significantly suppressed in *Ampk*$^{-/-}$ osteoblasts compared to

that of the controls (Fig. 7D-I). In contrast, the expressions of *Rankl* and *Rankl/Opg* ratio were significantly increased (Fig. 7J and L). Furthermore, we isolated BMSC from femur and examined the expressions of differentiation markers of osteoblasts. Real-time PCR showed that the expressions of *Osteocalcin* and *Bmp-2* were significantly suppressed in *Ampk*$^{-/-}$ BMSC compared to those of the controls (Fig. 8C and D). The expressions of *Alp*, *T1c*, and *Runx2* were tended to be decreased in *Ampk*$^{-/-}$ BMSC (Fig. 8A, B, and E), while *Rankl* and *Rankl/Opg* ratio were tended to be increased (Fig. 8G and I) although the differences did not reach significance. These findings indicate that disruption of *Ampkα1* inhibits the differentiation of osteoblasts and induces osteoclastogenesis by increasing RANKL expression.

Discussion

In the present study, we demonstrated that deletion of AMPKα1 in osterix-lineage cells impaired growth and bone development after birth and decreased trabecular and cortical bone volume. These findings indicate that osteoblast AMPK plays an important role in postnatal bone development. We and other researchers have previously shown that activation of AMPK stimulates the differentiation of osteoblasts (9–13), and, in the present study, we found that osteoblastic differentiation was significantly inhibited in primary cultured osteoblasts from *Ampk*$^{-/-}$ mice. We thus

295 hypothesized that the decreased bone volume of *Ampk*$^{-/-}$ mice may be caused by
296 inhibition of bone formation. Because histomorphometric analysis showed slightly
297 increased the number of osteoblasts and no change in bone formation rate, osteoblast
298 function might be attenuated by deletion of AMPK in osteoblasts. When the BFR was
299 examined at the endosteal and periosteal surface of cortical bone separately, BFR at the
300 endosteal surface was significantly decreased, while BFR at the periosteal surface was
301 significantly increased. These findings suggest that deletion of osteoblast AMPK
302 induced the suppression of osteoblast function and epiphyseal ossification although
303 osteoblasts at periosteal surface reciprocally activated. In contrast, the number of
304 osteoclasts was significantly increased in *Ampk*$^{-/-}$ mice. Taken together, these findings
305 suggest that osteoblastic AMPK plays important roles in bone formation as well as bone
306 turnover *in vivo*.

307 A previous study showed that conventional knockout of AMPKα1 in mice
308 decreased trabecular bone volume *in vivo* (12,17). In these mice, a significant increase
309 in bone resorption was found by histomorphometric analysis. The bone phenotype of
310 AMPKα1 knockout mice is similar to that of our *Ampk*$^{-/-}$ mice. Moreover, previous *in*
311 *vitro* studies showed that activation of AMPK significantly decreased the expression of
312 RANKL in osteoblasts (16). In the present study, we demonstrated that deletion of

AMPKα1 significantly increased the expression of *Rankl* and the ratio of *Rankl*/*Opg* in primary cultured osteoblasts from *Ampk*$^{-/-}$ mice compared to that of controls. Therefore, our present findings are consistent with previous studies suggesting that osteoblast AMPK plays an important role in the regulation of osteoclastogenesis and bone turnover by decreasing RANKL expression. In contrast, BFR was slightly, but not significantly, increased in the conventional AMPKα1 knockout mice (17). Because the present study showed no change in total BFR in our osteoblast-specific AMPKα1 knockout mice, it is suggested that AMPK in other cells might affect bone formation. We previously demonstrated that AMPK activation in osteocytes increased the expression of sclerostin (8), which inhibits osteoblast differentiation (21). This may explain the difference in BFR between conventional AMPKα1 knockout and ours. Further studies are thus necessary to investigate *in vivo* roles of osteocyte AMPK in bone.

It has been reported that several cytokines and drugs influence AMPK activation and regulate energy homeostasis. IGF-I is known to be involved in bone formation and remodeling, and it is reported that IGF-I modulates AMPK activity in various cell types (22). A recent study demonstrated that AMPK activation is required for the activation of IGF-I in early stages of osteoblast differentiation (23). Moreover,

331 Wang *et al*. reported that IGF-I receptor knockout mice generated by crossing Osx-Cre
332 transgenic mice showed postnatal bone growth retardation (24). Osteoblast-specific
333 IGF-I receptor null mice showed irregular morphology of the growth plate and lower
334 trabecular bone volume, accompanied by decreased chondrocyte proliferation and
335 differentiation, and decreased osteoblast differentiation; this bone phenotype is similar
336 to that of our *Ampk*$^{-/-}$ mice. Therefore, although the roles of osteoblast AMPK in IGF-I
337 signaling are still unclear, further studies are necessary to investigate whether AMPK
338 plays a role as a key molecule in hormonal regulation of bone modeling and
339 remodeling.

340 AMPK is considered as a major target molecule for diabetes mellitus, and
341 diabetes-related osteoporosis has become an important issue worldwide. Although the
342 pathophysiology of diabetes-related bone fragility is still unclear, previous studies
343 suggested that dysfunction of osteoblasts and low turnover of bone are involved (25).
344 We previously showed that metformin, an antidiabetic drug, stimulates the
345 differentiation and mineralization of osteoblastic MC3T3-E1 cells by activating AMPK
346 (10). In addition, other researchers have demonstrated that metformin inhibits RANKL
347 expression and stimulates OPG expression in osteoblasts; supernatants from cultured
348 osteoblasts treated with metformin significantly suppressed osteoclast formation and

expression of tartrate-resistant acid phosphatase and cathepsin K in osteoclasts (16), leading to an increase in bone mass. Indeed, several clinical studies suggested the beneficial effects of metformin on fracture risk in patients with type 2 diabetes mellitus (26,27). Thus, the results of this study may be understood to show the role of AMPK as the target molecule of metformin in bone, and suggest that AMPK activation may be a candidate for the treatment of diabetes-related osteoporosis.

Here, we examined the role of AMPK in osteoblast differentiation and bone development. However, previous *in vitro* studies have shown that AMPK plays a pivotal role in the commitment of multipotential mesenchymal stem cells to osteoblast lineage and adipocytes (28–30). Recently, Wang *et al.* demonstrated that AMPK hyperactivation induced by a lentivirus vector significantly stimulated osteoblastic MC3T3-E1 cell osteogenesis and inhibited 3T3-L1 cell adipogenesis (28,29). Chen *et al.* showed that AMPK activation by metformin activated the osteogenic transcription factor Runx2 and inactivated PPARγ (30), a master regulator of fat cell development. The present study showed that deletion of AMPK in Osx-expressing cells significantly decreased the expression of Runx2 and osterix, although osteoblast number and bone formation were not affected. Because Runx2 and osterix are reported to counteract PPARγ-mediated adipogenesis (31,32), it would be interesting to examine the effect of AMPK deletion in

Osx-expressing cells on bone marrow adiposity in future.

In conclusion, the present study showed that deletion of osteoblast AMPK induced retardation of postnatal bone development, as well as reduction in trabecular and cortical bone volume, by decreasing osteoblast differentiation and increasing RANKL expression. These findings suggest that osteoblast AMPK plays important roles in bone modeling and remodeling. Accordingly, activation of osteoblast AMPK may be a candidate for treatment of osteoporosis with high bone turnover, as well as diabetes-related osteoporosis, although further studies are necessary to clarify the roles of AMPK in bone.

Acknowledgements

This study was partly supported by a Grant-in-Aid for Scientific Research (C) (15K09433). Authors' roles: Study design and conduct: IK and TS. Performed the experiments and analyzed the data: IK and AT. Contributed equipment/materials: IK, KT, MN, and TS. Wrote the paper: IK. Approved the final version: all authors. IK takes responsibility for the integrity of the data analysis. The authors thank Keiko Nagira for technical assistance.

Conflicts of interest

None.

References

1. Kahn BB, Alquier T, Carling D, Hardie DG. AMP-activated protein kinase: ancient energy gauge provides clues to modern understanding of metabolism. Cell Metab 2005; 1: 15-25.
2. Ruderman NB, Carling D, Prentki M, Cacicedo JM. AMPK, insulin resistance, and the metabolic syndrome. J Clin Invest 2013; 123: 2764-2772.
3. Scott JW, Oakhill JS, van Denderen BJ. AMPK/SNF1 structure: a menage a trios of energy-sensing. Front Biosci 2009; 14: 596-610.
4. Motoshima H, Goldstein BJ, Igata M, Araki E. AMPK and cell proliferation-AMPK as a therapeutic target for atherosclerosis and cancer. J Physiol 2006; 574: 63-71.
5. Salminen A, Hyttinen JM, Kaarniranta K. AMP-activated protein kinase inhibits NF-κB signaling and inflammation: impact on health span and lifespan. J Mol Med 2011; 89: 667-676.
6. Jeyabalan J, Shah M, Viollet B, Chenu C. AMP-activated protein kinase pathway and bone metabolism. J Endocrinol 2012; 212: 277-290.
7. Quinn JM, Tam S, Sims NA, Saleh H, McGregor NE, Poulton IJ, Scott JW, Gillespie MT, Kemp BE, van Denderen BJ. Germline deletion of AMP-activated protein kinase beta subunits reduces bone mass without altering osteoclast

406 differentiation or function. FASEB J 2010; 24: 275-285.
407 8. Yokomoto-Umakoshi M, Kanazawa I, Takeno A, Tanaka K, Notsu M, Sugimoto T.
408 Activation of AMP-activated protein kinase decreases receptor activator of NF-κB
409 ligand expression and increases sclerostin expression by inhibiting the mevalonate
410 pathway in osteocytic MLO-Y4 cells. Biochem Biophys Res Commun 2016; 469:
411 791-796.
412 9. Kanazawa I, Yamaguchi T, Yano S, Yamauchi M, Yamamoto M, Sugimoto T.
413 Adiponectin and AMP kinase activator stimulate proliferation, differentiation, and
414 mineralization of osteoblastic MC3T3-E1 cells. BMC Cell Biol 2007; 8: 51.
415 10. Kanazawa I, Yamaguchi T, Yano S, Yamauchi M, Sugimoto T. Metformin enhances
416 the differentiation and mineralization of osteoblastic MC3T3-E1 cells via AMP
417 kinase activation as well as eNOS and BMP-2 expression. Biochem Biophys Res
418 Commun 2008; 375: 414-419.
419 11. Kanazawa I, Yamaguchi T, Yano S, Yamauchi M, Sugimoto T. Activation of AMP
420 kinase and inhibition of Rho kinase induce the mineralization of osteoblastic
421 MC3T3-E1 cells through endothelial NOS and BMP-2 expression. Am J Physiol
422 Endocrinol Metab 2009; 296: E139-146.
423 12. Shah M, Kola B, Bataveljic A, Arnett TR, Viollet B, Saxon L, Korbonits M, Chenu

C. AMP-activated protein kinase (AMPK) activation regulates in vitro bone formation and bone mass. Bone 2010; 47: 309-319.

13. Jang WG, Kim EJ, Lee KN, Son HJ, Koh JT. AMP-activated protein kinase (AMPK) positively regulates osteoblast differentiation via induction of Dlx5-dependent Runx2 expression in MC3T3E1 cells. Biochem Biophys Res Commun 2011; 404: 1004-1009.

14. Lee YS, Kim YS, Lee SY, Kim GH, Kim BJ, Lee SH, Lee KU, Kim GS, Kim SW, Koh JM. AMP kinase acts as a negative regulator of RANKL in the differentiation of osteoclasts. Bone 2010; 47: 926-937.

15. Kang H, Viollet B, Wu D. Genetic deletion of catalytic subunits of AMP-activated protein kinase increases osteoclasts and reduces bone mass in young adult mice. J Biol Chem 2013; 288: 12187-12196.

16. Mai QG, Zhang ZM, Xu S, Lu M, Zhou RP, Zhao L, Jia CH, Wen ZH, Jin DD, Bai XC. Metformin stimulates osteoprotegerin and reduces RANKL expression in osteoblasts and ovariectomized rats. J Cell Biochem 2011; 112: 2902-2909.

17. Jeyabalan J, Shah M, Viollet B, Roux JP, Chavassieux P, Korbonits M, Chenu C. Mice lacking AMP-activated protein kinase α1 catalytic subunit have increased bone remodelling and modified skeletal responses to hormonal challenges induced

442 by ovariectomy and intermittent PTH treatment. J Endocrinol 2012; 214: 349-358.
443 18. Nakada D, Saunders TL, Morrison SJ. Lkb1 regulates cell cycle and energy
444 metabolism in haematopoietic stem cells. Nature 2010; 468: 653-658.
445 19. Rodds SJ, McMahon AP. Distinct roles for Hedgehog and canonical Wnt signaling
446 in specification, differentiation and maintenance of osteoblast progenitors.
447 Development 2006; 133: 3231-3244.
448 20. Kanazawa I, Canaff L, Abi Rafeh J, Angrula A, Li J, Riddle RC, Boraschi-Diaz I,
449 Komarova SV, Clemens TL, Murshed M, Hendy GN. Osteoblast menin regulates
450 bone mass in vivo. J Biol Chem 2015; 290: 3910-3924.
451 21. Li X, Zhang Y, Kang H, Liu W, Liu P, Zhang J, Harris SE, Wu D. Sclerostin binds
452 to LRP5/6 and antagonizes canonical Wnt signaling. J Biol Chem 2005; 280:
453 19883-19887.
454 22. Tulipano G, Faggi L, Sibilia V, Giustina A. Points of integration between the
455 intracellular energy sensor AMP-activated protein kinase (AMPK) activity and the
456 somatotroph axis function. Endocrine 2012; 42: 292-298.
457 23. Xi G, Rosen CJ, Clemmons DR. IGF-I and IGFBP-2 stimulate AMPK activation
458 and autophagy, which are required for osteoblast differentiation. Endocrinology
459 2016; 157: 268-281.

460 24. Wang Y, Menendez A, Fong C, ElAlieh HZ, Kubota T, Long R, Bikle DD. IGF-I
461 signaling in osterix-expressing cells regulates secondary ossification center
462 formation, growth plate maturation, and metaphyseal formation during postnatal
463 bone development. J Bone Miner Res 2015; 30: 2239-2248.
464 25. Starup-Linde J, Eriksen SA, Lykkeboe S, Handberg A, Vestergaard P. Biochemical
465 markers of bone turnover in diabetes patients--a meta-analysis, and a
466 methodological study on the effects of glucose on bone markers. Osteoporos Int
467 2014; 25: 1697-1708.
468 26. Vestergaard P, Rejnmark L, Mosekilde L. Relative fracture risk in patients with
469 diabetes mellitus, and the impact of insulin and oral antidiabetic medication on
470 relative fracture risk. Diabetologia 2005; 48: 1292-1299.
471 27. Melton LJ 3rd, Leibson CL, Achenbach SJ, Themeau TM, Khosla S. Fracture risk in
472 type 2 diabetes: Update of a population-based study. J Bone Miner Res 2008; 23:
473 1334-1342.
474 28. Wang YG, Qu XH, Yang Y, Han XG, Wang L, Qiao H, Fan QM, Tang TT, Dai KR.
475 AMPK promotes osteogenesis and inhibits adipogenesis through AMPK-Gfi1-OPN
476 axis. Cell Signal 2016; 28: 1270-1282.
477 29. Wang YG, Han XG, Yang Y, Qiao H, Dai KR, Fan QM, Tang TT. Functional

differences between AMPK α1 and α2 subunits in osteogenesis, osteoblast-associated induction of osteoclastogenesis, and adipogenesis. Sci Rep 2016; 6: 32771.

30. Chen SC, Brooks R, Houskeeper J, Bremner SK, Dunlop J, Viollet B, Logan PJ, Salt IP, Ahmed SF, Yarwood SJ. Metformin suppresses adipogenesis through both AMP-activated protein kinase (AMPK)-dependent and AMPK-independent mechanisms. Mol Cell Endocrinol 2017; 440: 57-68.

31. Han Y, Kim CY, Cheong H, Lee KY. Osterix represses adipogenesis by negatively regulating PPARγ transcriptional activity. Sci Rep 2016; 6: 35655.

32. Enomoto H, Furuichi T, Zanma A, Yamana K, Yoshida C, Sumitani S, Yamamoto H, Enomoto-Iwamoto M, Iwamoto M, Komori T. Runx2 deficiency in chondrocytes causes adipogenic changes in vitro. J Cell Sci 2004; 117: 417-425.

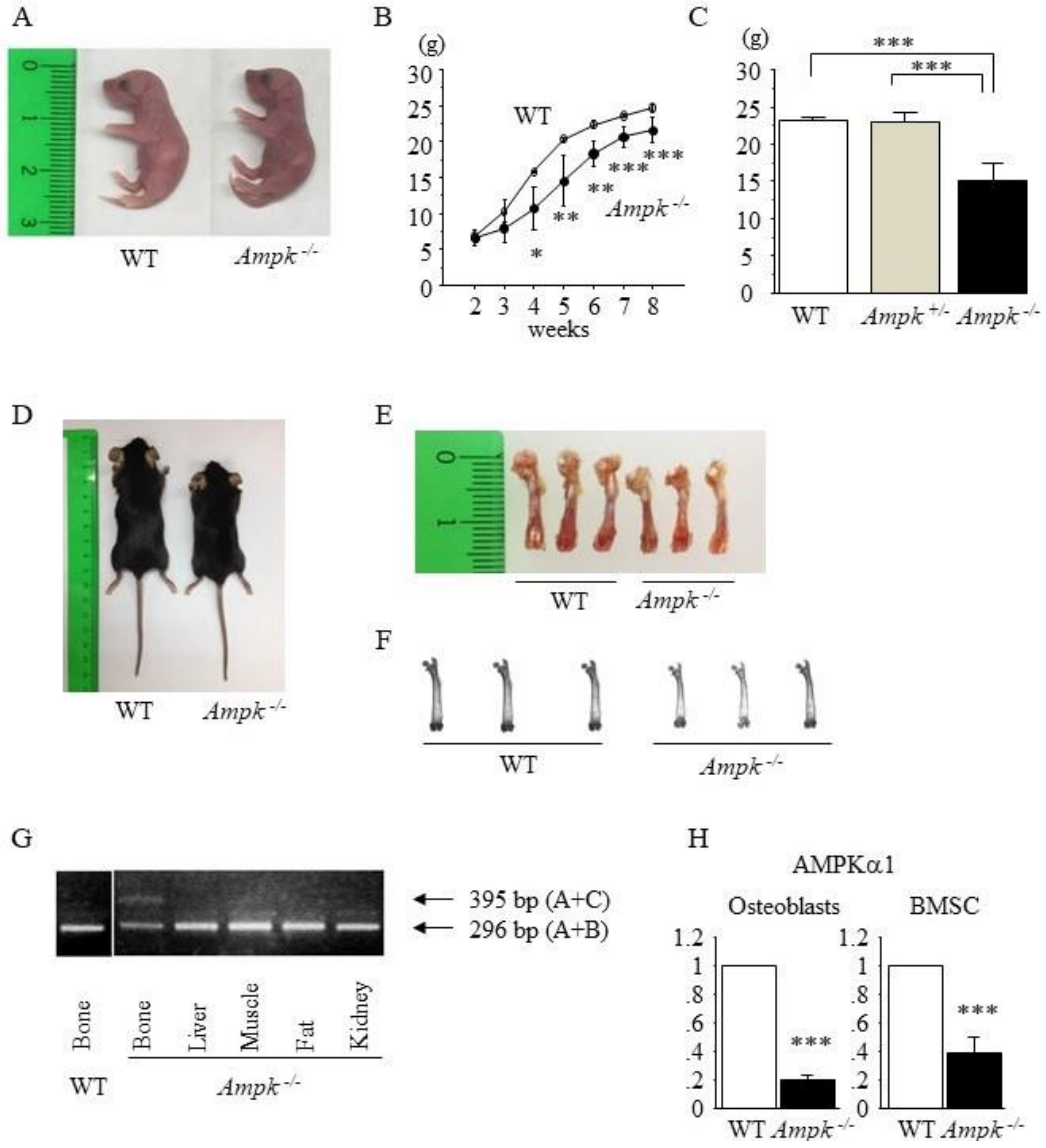

Fig. 1 Growth retardation in *Ampk*$^{-/-}$ mice during postnatal development

Representative pictures of body size at birth (A). Growth curve from 2 weeks to 8 weeks after birth (n = 6 per strain) (B), and body weight at 8 weeks (n = 6) (C). Representative pictures of body size (D), femurs (E), and X-ray films of femurs (F) at 8 weeks. PCR analyses of genomic DNA extracted from different tissues from *Ampk*$^{-/-}$ and WT mice with primers amplifying the excised region (Δ3 *Ampk* allele, 395 bp;

498 wild-type *Ampk* allele, 296 bp) (G). The expression of AMPKα1 in primary osteoblasts
499 isolated from calvaria and BMSC from femur was examined by real-time PCR (H) (n =
500 4). Gene expression was normalized to that of 36B4, a housekeeping gene. ∗p < 0.05,
501 ∗∗p < 0.01, ∗∗∗p<0.001.

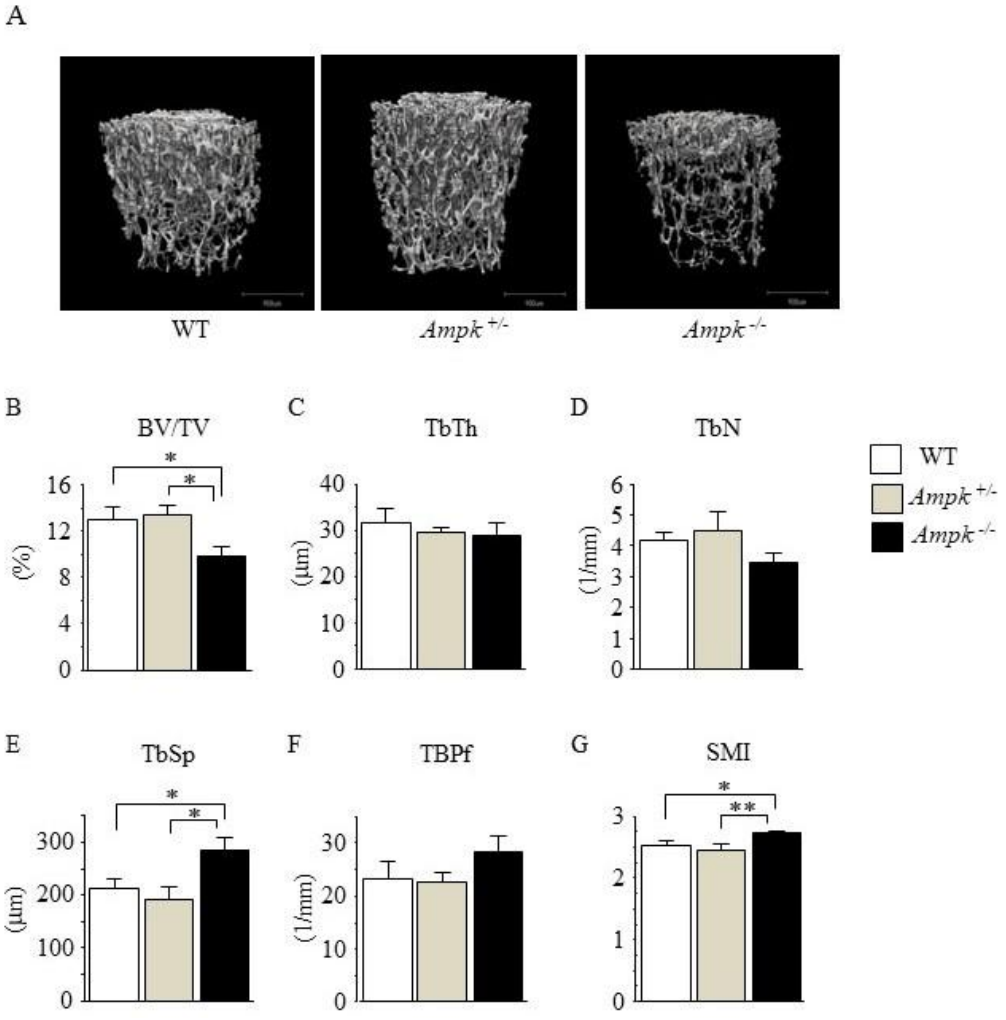

502

503 **Fig. 2 Reduction in trabecular bone volume in *Ampk*$^{-/-}$ mice by μCT**

504 Representative images of μCT analysis (A) and trabecular bone parameters of
505 distal femurs (B-G) from 8-week-old mice (n = 6 per strain). White boxes indicate WT,

gray boxes indicate *Ampk*$^{+/-}$ and black boxes indicate *Ampk*$^{-/-}$ mice. BV, bone volume; TV, tissue volume; TbTh, trabecular thickness; TbN, trabecular number; TbSp, trabecular separation; TBPf, trabecular bone pattern factor; SMI, structure model index. $*p < 0.05$, $**p < 0.01$.

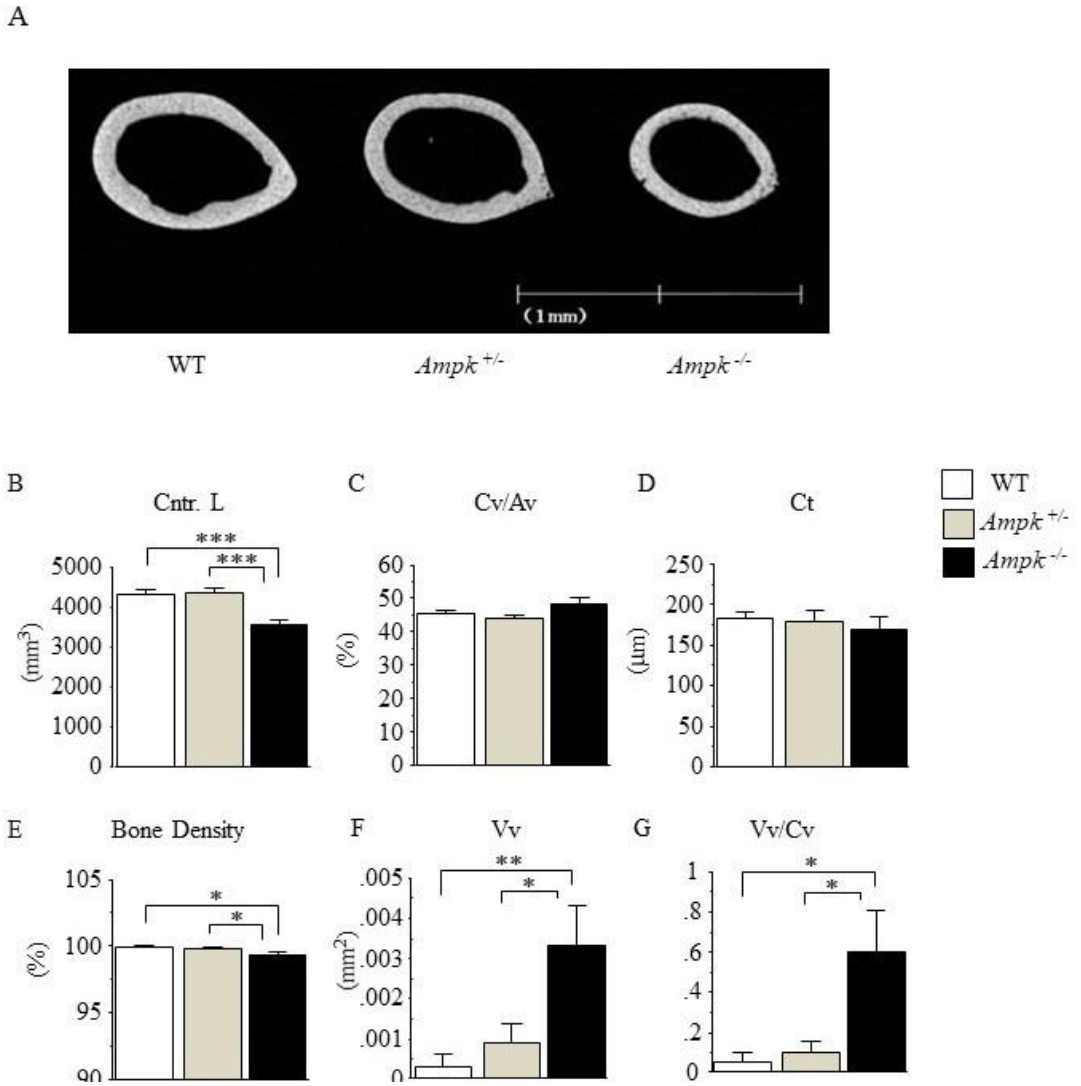

Fig. 3 Decreased cortical bone size and increased cortical vessel volume in *Ampk*$^{-/-}$ mice by μCT

Representative images of μCT analysis (A) and cortical bone parameters of

femurs (B-G) from 8-week-old *Ampk*$^{-/-}$ mice and controls (n = 4 per strain). White boxes indicate WT, gray boxes indicate *Ampk*$^{+/-}$ and black boxes indicate *Ampk*$^{-/-}$ mice. Cntr. L, center line length; Cv, cortical bone volume; Av, all bone volume; Ct, mean cortical bone thickness; Vv, vessel volume. ∗p < 0.05, ∗∗p < 0.01, ∗∗∗p<0.001.

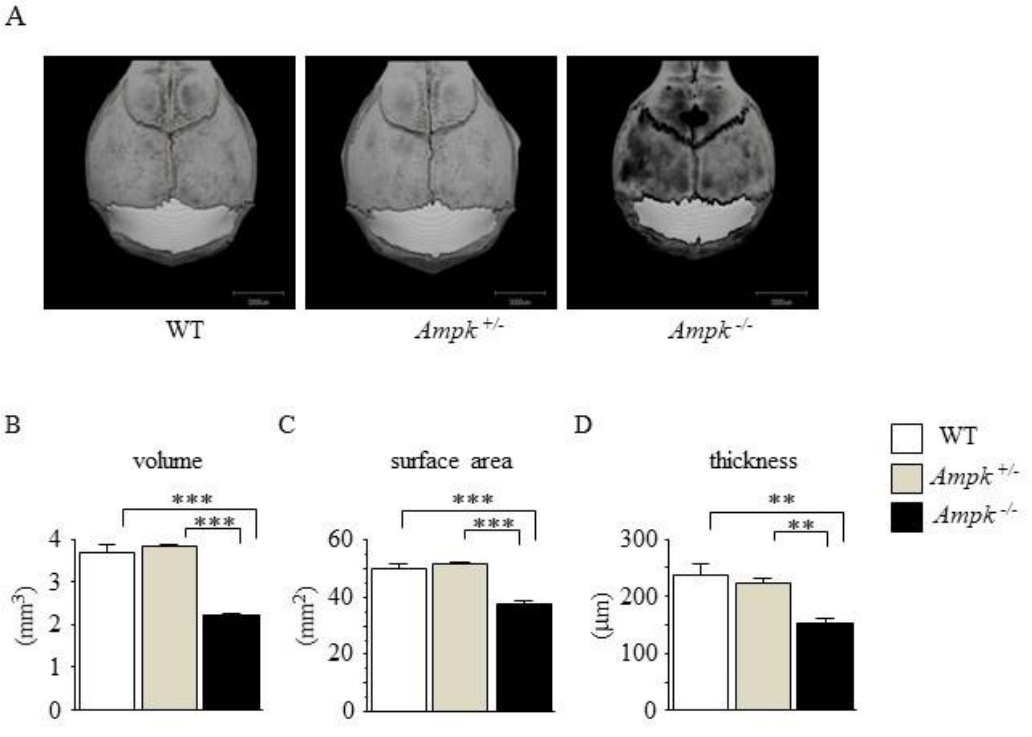

Fig. 4 Developmental defects in skull in *Ampk*$^{-/-}$ mice by μCT

Representative images of μCT analysis (A). Volume (B), surface area (C), and thickness (D) were measured and compared among WT, *Ampk*$^{+/-}$, and *Ampk*$^{-/-}$ mice. White boxes indicate WT, gray boxes indicate *Ampk*$^{+/-}$ and black boxes indicate *Ampk*$^{-/-}$ mice. ∗∗p < 0.01, ∗∗∗p<0.001.

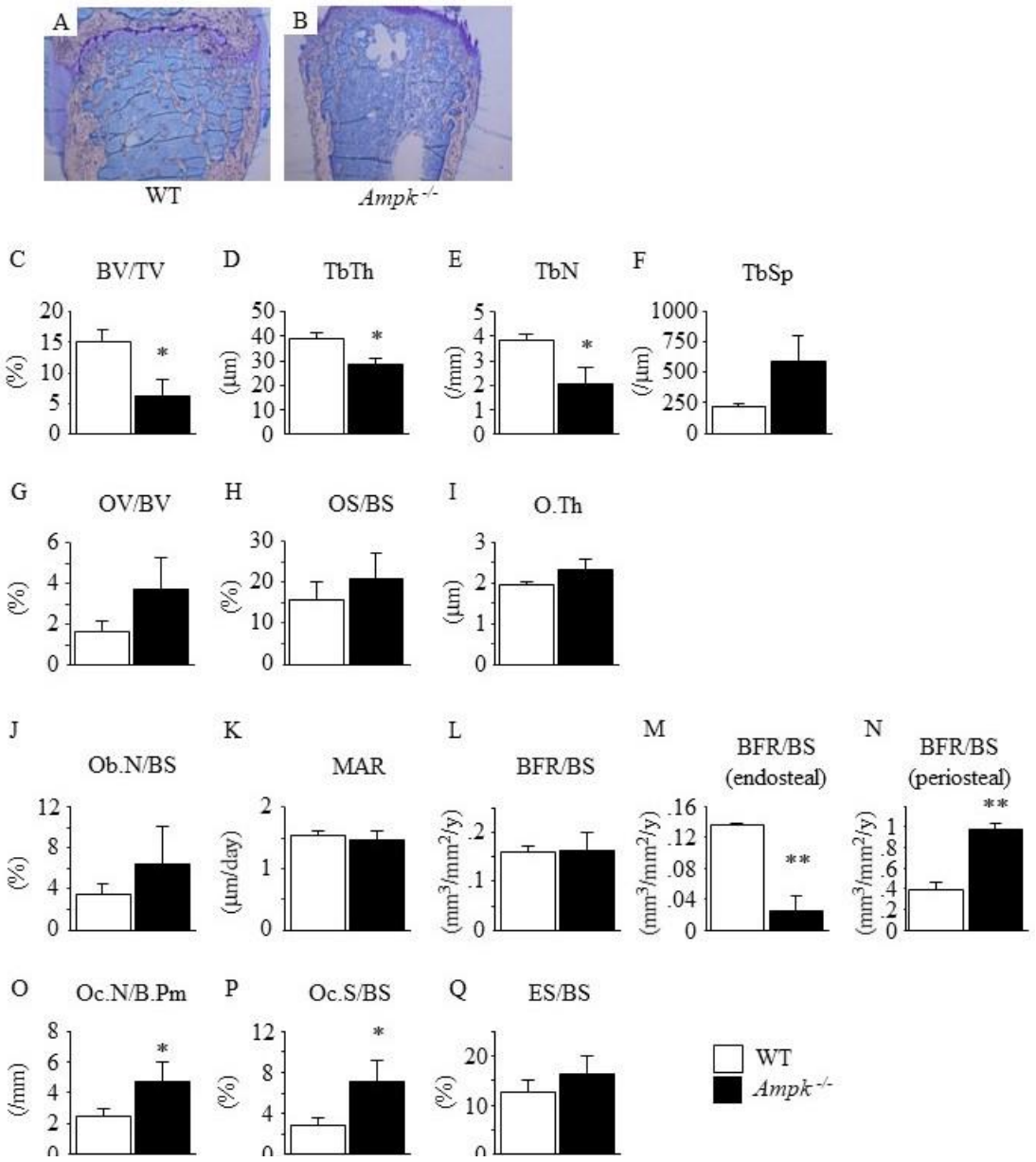

Fig. 5 Reduction in trabecular bone volume in *Ampk*$^{-/-}$ mice by histomorphometric analysis

Representative pictures of toluidine blue staining (A), and trabecular bone parameters of distal femurs (C-O) from 8-week-old *Ampk*$^{-/-}$ mice and WT (n = 4 per strain). White boxes indicate WT and black boxes indicate *Ampk*$^{-/-}$ mice. BV, bone

volume; TV, tissue volume; TbTh, trabecular thickness; TbN, trabecular number; TbSp, trabecular separation; OV, osteoid volume; OS, osteoid surface; BS, bone surface; O.Th, osteoid thickness; Ob.N, osteoblast number; MAR, mineral apposition rate; BFR, bone formation rate; Oc.N osteoclast number; Oc.S, osteoclast surface; ES, eroded surface. *p < 0.05, **p < 0.01.

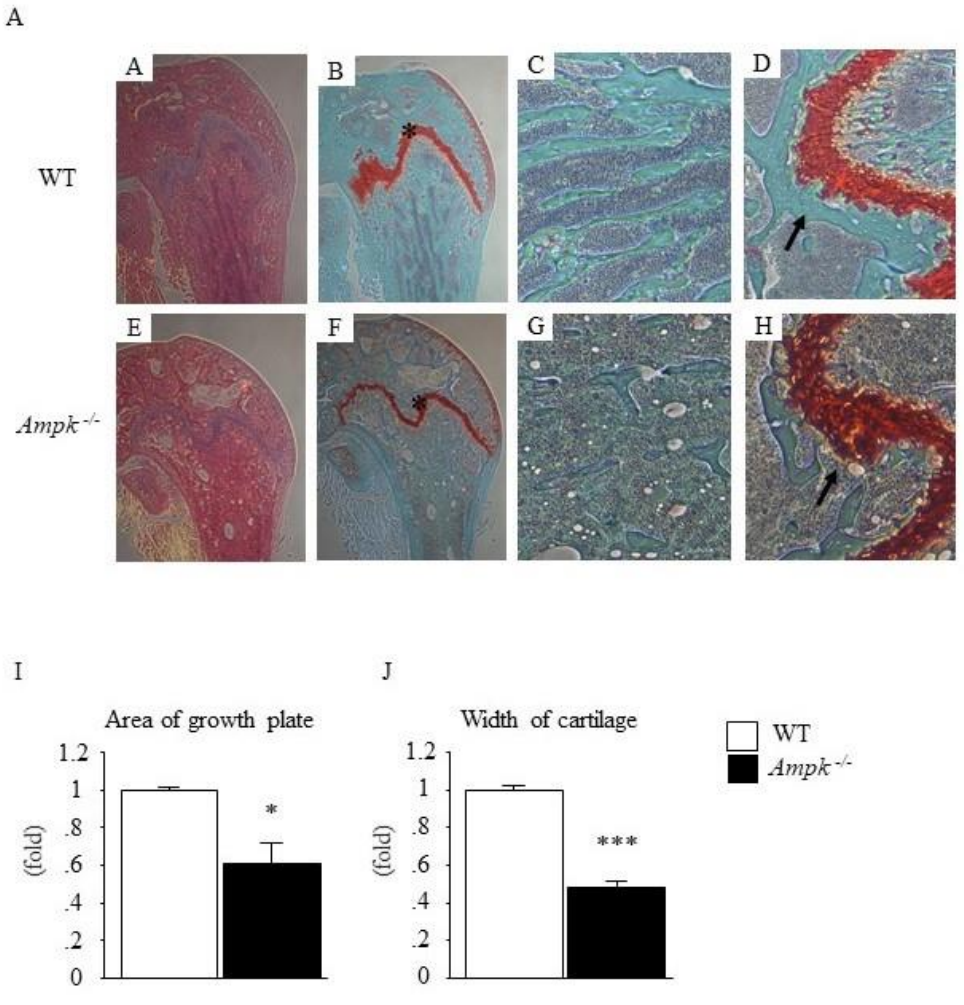

Fig. 6 Abnormal skeletal morphology in *Ampk*$^{-/-}$ mice

Representative pictures of H&E staining (A and E) and Safranin O staining (B-D and F-H) of distal femurs from 8-week-old *Ampk*$^{-/-}$ mice and WT. Asterisks

indicate growth plate. Arrows indicate cartilage adjacent to the growth plate. Area of growth plate (I) and mean width of cartilage adjacent to the growth plate (J) were measured and compared.

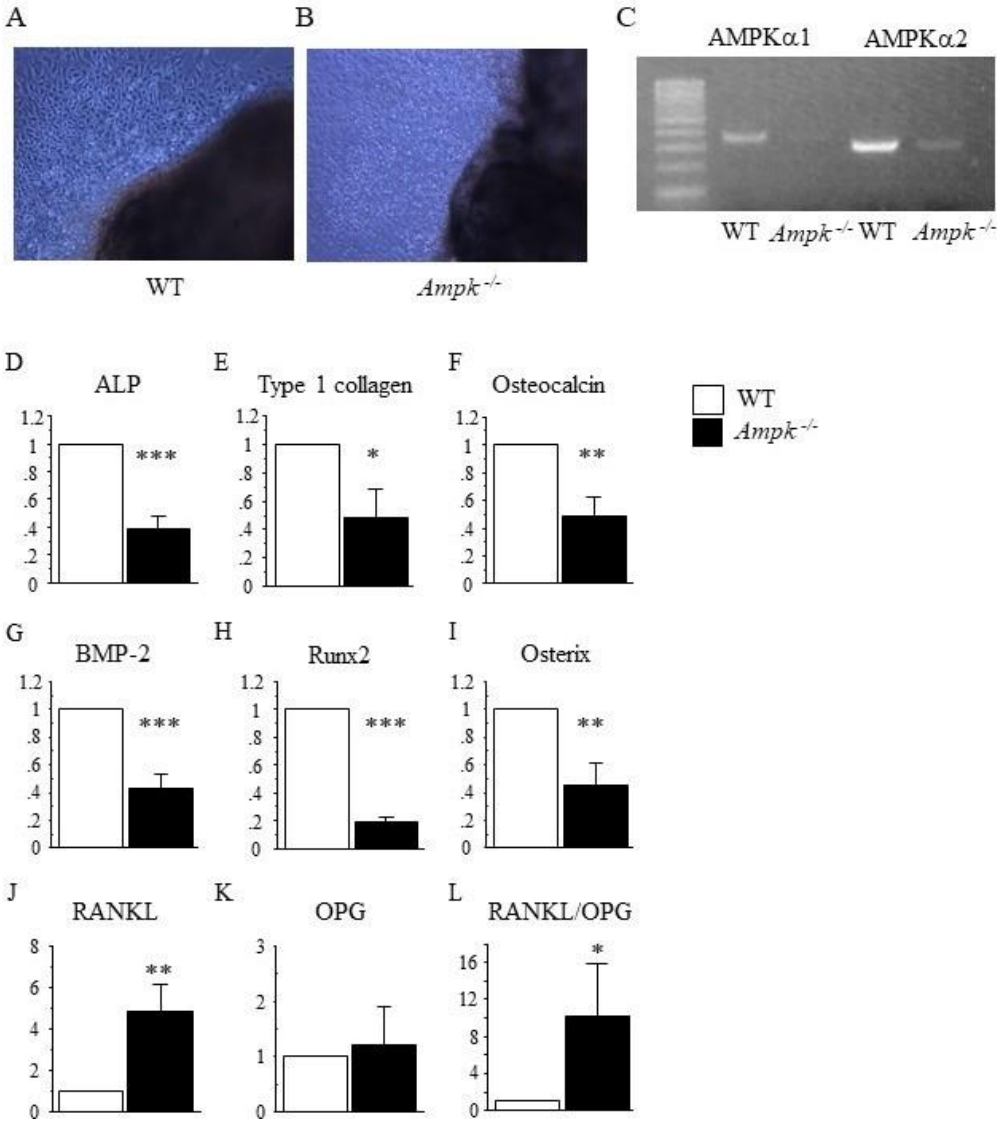

Fig. 7 Effects of deletion of *Ampkα1* in isolated primary osteoblasts

Representative pictures of isolated osteoblasts (A and B). Total RNA from the isolated osteoblasts was subjected to RT-PCR, and the PCR products were visualized in

547 a 1.8% agarose gel stained with ethidium bromide (C). The expression of alkaline
548 phosphatase (ALP), type 1 collagen, osteocalcin, bone morphogenetic protein-2
549 (BMP-2), Runx2, osterix, receptor activator of nuclear kappa-B ligand (RANKL), and
550 osteoprotegerin (OPG) was examined by real-time PCR (D-L) (n = 6). Gene expression
551 was normalized to that of 36B4, a housekeeping gene. White boxes indicate WT and
552 black boxes indicate *Ampk*$^{-/-}$ mice. *p < 0.05, **p < 0.01, ***p < 0.001.

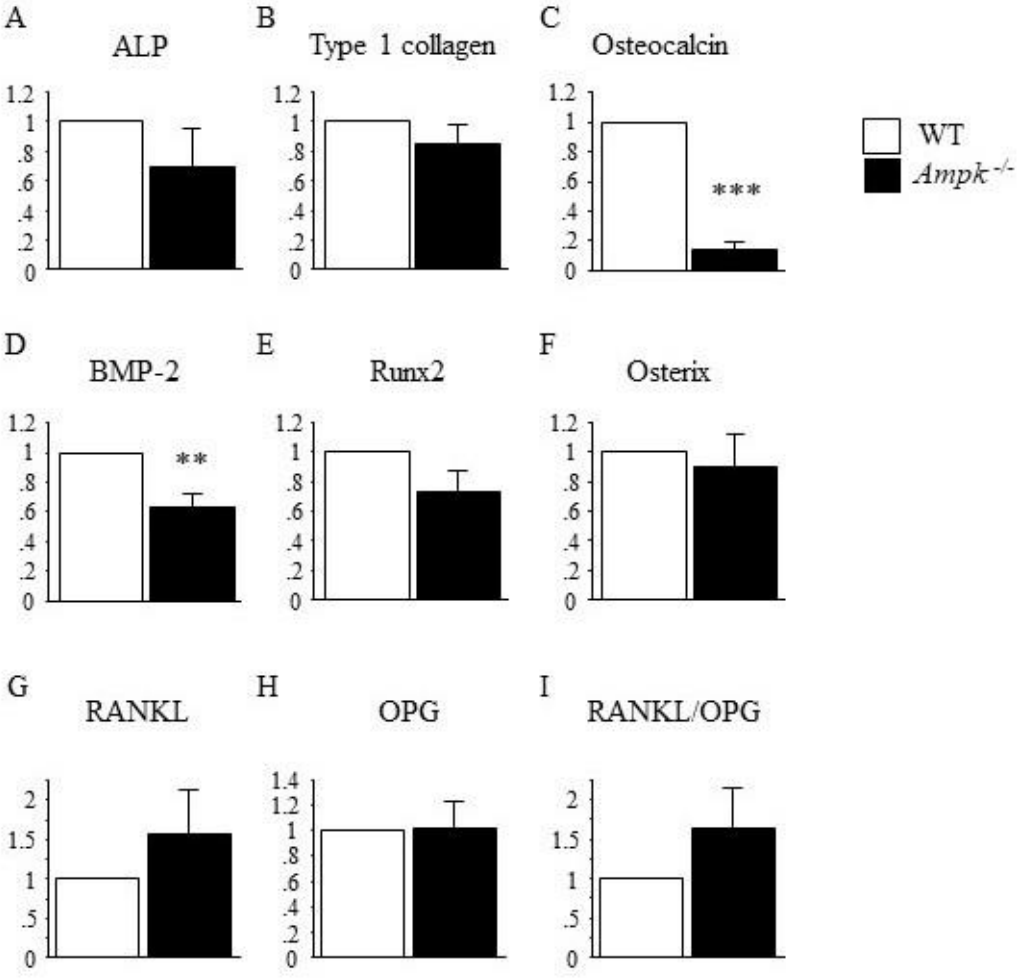

553

554 **Fig. 8 Effects of deletion of *Ampkα1* in isolated BMSC**

555 The expression of alkaline phosphatase (ALP), type 1 collagen, osteocalcin,

556 bone morphogenetic protein-2 (BMP-2), Runx2, osterix, receptor activator of nuclear
557 kappa-B ligand (RANKL), and osteoprotegerin (OPG) was examined by real-time PCR
558 (A-I) (n = 4). Gene expression was normalized to that of 36B4, a housekeeping gene.
559 White boxes indicate WT and black boxes indicate *Ampk*$^{-/-}$ mice. **p < 0.01, ***p <
560 0.001.
561